Theory of magnetization in multiferroics: Competition between ferromagnetic and antiferromagnetic domains

Helen V. Gomonay,[1,2,*] Ievgeniya G. Korniienko,[1] and Vadim M. Loktev[1,2]
[1]*National Technical University of Ukraine "KPI," ave Peremogy, 37, 03056 Kyiv, Ukraine*
[2]*Bogolyubov Institute for Theoretical Physics NAS of Ukraine, Metrologichna strasse 14-b, 03680, Kyiv, Ukraine*
(Received 16 March 2010; revised manuscript received 4 January 2011; published 22 February 2011)

Many technological applications of multiferroics are based on their ability to reconstruct the domain structure (DS) under the action of small external fields. In the present paper we analyze the different scenarios of the DS behavior in a multiferroic that shows simultaneously ferromagnetic and antiferromagnetic ordering on the different systems of magnetic ions. We consider the way to control a composition of the DS and macroscopic properties of the sample by an appropriate field treatment. It is found that the sensitivity of the DS to the external magnetic field and the magnetic susceptibility in a low-field region are determined mainly by the de-stressing effects (that have a magnetoelastic origin). In a particular case of the $Sr_2Cu_3O_4Cl_2$ crystal we anticipate the peculiarities of the elastic and magnetoelastic properties at $T \approx 100$ K.

DOI: 10.1103/PhysRevB.83.054424 PACS number(s): 75.85.+t, 75.60.Ch, 46.25.Hf, 75.50.Ee

I. INTRODUCTION

During the las decade special attention was paid to the materials in which magnetism coexisted with the other types of ordering (i.e., ferroelectric,[1,2] elastic,[3] or martensitic[4]). Solids that show strong coupling between the different types of ordering are often called multiferroics.[5] A growing interest in multiferroics is based on the possibility (i) to control such macroscopic properties of a sample as conductivity, magnetization, or elongation, with the suitable fields of a different nature; and (ii) to manipulate the state of the magnetically (electrically, etc.) inert materials (see, e.g., Refs. 6 and 7).

One of the most technologically appealing properties of multiferroics, namely, the sensitivity of their macroscopic properties to the influence of small external fields, is due to the formation and reconstruction of the domain structure (DS).[8–10] This adaptivity, or ability to change macroscopic parameters (such as a shape, magnetization, or electric polarization) in response to external forces, is related to the finite size and boundary of the sample. However, the description of the DS in multiferroics seems to be a very complicated problem mostly due to the fact that the domains can have different origins and the corresponding DS is governed by different physical mechanisms;[11] domain walls that separate different types of domains can clamp each other;[12] the domains of different natures appear at different spatial scales[13] and thus form a hierarchical structure. For example, the DS of some popular magnetoelectrics [such as $BiFeO_3$, $BaTiO_3$ (Refs. 6, 14 and 15), $MnWO_4$ (Ref. 16), and $CuFe_{1-x}Ga_xO_2$ (Ref. 17)] consists of at least three types of axial domains with different antiferromagnetic (AFM) ordering and, in addition, two types of polar domains that differ in the orientation of ferroelectric polarization. While the appearance of equilibrium polar (magnetic or ferroelectric) DS can be explained by the well-known demagnetizing/depolarizing effects,[18] the thermodynamic equilibrium configuration of the axial domains needs special treatment because (i) AFM's produce no (or very small, in the case of weak ferromagnetics) demagnetizing fields, and (ii) axial (non-180°) domains usually show ferroelastic properties due to nonzero piezoelectric or/and magnetoelastic effects (see, e.g., Ref. 19). Moreover, both polar and ferroelastic domains can be sensitive to the same external field (electric or magnetic), but should, in general, show a different susceptibility related to the different nature of field-to-order parameter coupling.

In the present paper we address the questions "What will be the field-induced behavior of such a combined equilibrium DS in multiferroics? Can one observe some new features, caused by competition between the polar and axial (ferroelastic) domains?"

As the simplest example of the competing domains of a different nature we consider rather exotic multiferroics that show simultaneously ferromagnetic (FM) and AFM ordering on the different sites of the Brave lattice, namely, high-temperature superconducting systems (like $Sr_2Cu_3O_4Cl_2$ or $Ba_2Cu_3O_4Cl_2$). In contrast to magnetoelectrics like $BiFeO_3$ or $RMnO_3$, these systems have a relatively simple, nonhierarchial DS that includes a maximum of four types of domains. Such FM + AFM multiferroics should be distinguished from the systems with the intermediate state represented by a mixture of AFM and FM domains (like those observed in Refs. 20 and 21) that can be well described by demagnetizing effects.[22] In the present paper we analyze the competition between the FM and AFM domains using the concept of the shape-dependent de-stressing energy[23] that accounts for the long-range field of internal stresses induced by the transition into a magnetically ordered state. We concentrate our attention on the long-range dipole-dipole interactions between domains and neglect the direct contribution from the domain walls (which is responsible for the details of the domain pattern[24,25] and kinetics of relaxation processes). However, we implicitly take into account the mobility of the domain walls and difference in nucleation barriers for different types of domains.

In the framework of the phenomenological approach, we calculate the possible magnetization curves that can be obtained for the samples of different shape and different field treatment. On the basis of the developed model we make an attempt to interpret the unusual behavior of macroscopic magnetization observed in the experiments of Parks *et al.*[26] and

predict a peculiarity of the elastic properties of $Sr_2Cu_3O_4Cl_2$ at the temperature $T \approx 100$ K.

II. MODEL

The crystal structure of high-temperature superconducting cuprates $Sr_2Cu_3O_4Cl_2$ and $Ba_2Cu_3O_4Cl_2$ consists of Cu_3O_4 planes separated by spacer layers of SrCl or BaCl (Refs. 26–28). Two types of magnetic ions, CuI and CuII (see Fig. 1) form two interpenetrating square lattices within Cu_3O_4 planes. Within the temperature interval $T_{II} \approx 40$ K$\leqslant T \leqslant T_I \approx 380$ K the ions of the first type (CuI) are AFM ordered while the ions of the second type (CuII) bear a small but nonzero FM moment.[29] According to the experiments,[30] the mutual orientation of CuI and CuII moments depends upon the direction of the external magnetic field and can be either perpendicular or parallel. Thus, the magnetic structure consists of two weakly coupled subsystems, namely, an AFM, localized on CuI ions, and a FM one, localized on CuII ions. The FM subsystem is unambiguously described by the magnetization vector $\mathbf{M}_F$ and the AFM subsystem is described by two vectors: AFM vector $\mathbf{L} = (\mathbf{S}_1 - \mathbf{S}_2 + \mathbf{S}_3 - \mathbf{S}_4)/4$ and FM vector $\mathbf{M} = \sum_j \mathbf{S}_j/4$ (numeration of CuI sites is shown in Fig. 1).

In the absence of the external field the FM moments at CuII sites are oriented along ⟨110⟩ crystal directions perpendicular to the staggered magnetizations of the AFM subsystem, as shown in Fig. 1. Due to the tetragonal symmetry of the crystal (space group $I4/mmm$) an equilibrium magnetic structure can be realized in four types of equivalent domains as shown in Figs. 1 and 2. Domains of type A and B can be thought of as AFM domains because they correspond to different orientations of the $\mathbf{L}$ vector and thus are sensitive to the orientation of the magnetic field $\mathbf{H}$ with respect to the crystal axes (see Fig. 3). Types A1 and A2 (and, correspondingly, B1 and B2) are FM domains, they have an opposite direction from the $\mathbf{M}_F$ vector and can be removed from the sample by $\mathbf{H} \| \mathbf{M}_F$.

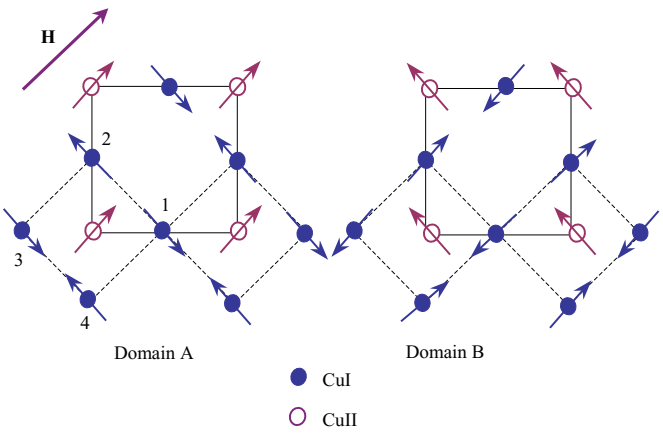

FIG. 1. (Color online) Magnetic structure of Cu_3O_4 layer in two different configurations (domains). Magnetic field is parallel to ⟨110⟩. Two types of magnetic ions are represented with the filled and hollow circles. FM ordered moments of CuII could be (a) parallel (domain A) or (b) perpendicular (domain B) to the applied magnetic field. Small canting of the CuI spins induced by the external magnetic field is ignored.

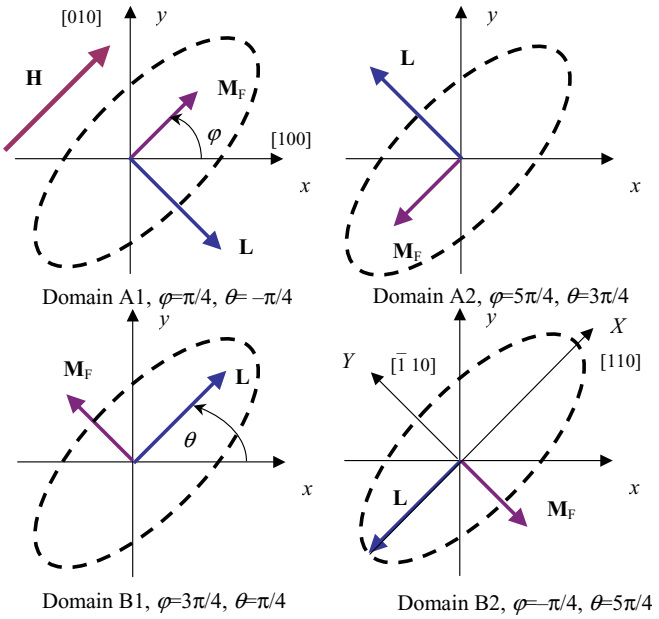

FIG. 2. (Color online) Four types of magnetic domains. Axes x and y are parallel to ⟨100⟩ crystal directions. The external magnetic field $\mathbf{H} \| [110]$ (if any). Types A and B have different orientations of AFM vector, types 1 and 2 correspond to opposite directions of FM vector $\mathbf{M}_F$. Ellipse (dashed line) images the supposed shape of the sample and its orientation (axes X, Y) with respect to crystal axes.

Qualitatively, the difference between the behavior of FM and AFM domains in the external magnetic field and the peculiarities of the possible magnetization curves is illustrated in Fig. 3. The structure consisting of FM domains reconfigures in the magnetic field which is parallel to an easy axis and does not change if the magnetic field is perpendicular to this axis. Macroscopic magnetization of the sample (and hence, macroscopic susceptibility) is inversely proportional to the appropriate component of the demagnetization tensor. In contrast, AFM domain structure reconfigures for both mutually perpendicular orientations of the magnetic field. Macroscopic magnetization depends upon the components of the de-stressing tensor that have a magnetoelastic origin. So, a material that bears simultaneously the features of FM and AFM can show some new type of behavior in the external magnetic field governed by competition between the demagnetizing and de-stressing effects.

The phenomenological description of the DS is based on the analysis of the free energy potential Φ of the sample. We take into account three constituents of Φ: magnetic Φ_{mag}, stray (demagnetizing) Φ_{stray}, and de-stressing Φ_{dest} energies

$$\Phi = \Phi_{mag} + \Phi_{stray} + \Phi_{dest}. \quad (1)$$

The last contribution describes shape-induced effects related with AFM ordering. Usually, in FM (and also weak FM) this term is not included into consideration because all the shape-induced effects are accounted through the magnetic stray energy Φ_{stray}. However, in multiferroics with AFM ordering, the contribution of the de-stressing energy is important and gives rise to qualitatively new effects as will be shown below.

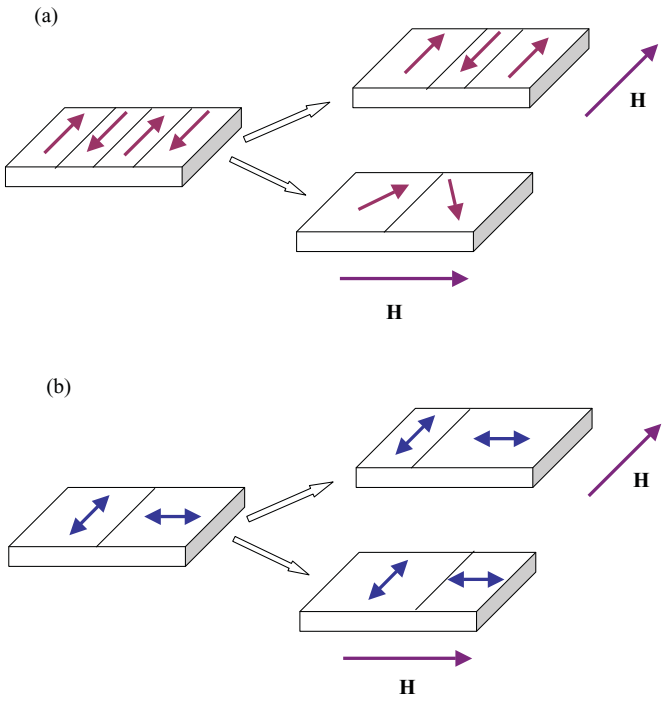

FIG. 3. (Color online) Behavior of the (a) FM and (b) AFM domain structures in the external magnetic field **H**. In the absence of field, both types of domains (shown by arrows) are equally represented. (a) FM domains have the opposite direction of the magnetization vector. The magnetic field applied parallel to an easy axis (upper panel) removes the degeneracy of the domains. As a result, a fraction of the favorable domain increases. If **H** is perpendicular to the easy axis (lower panel), domains of both types are equivalent, the domain fraction does not change, and magnetic field induces a tilt of the magnetizations. (b) AFM domains have different (perpendicular) orientations of AFM vectors. Degeneracy of the domains is removed for any of two mutually perpendicular orientations of the magnetic field.

The magnetic energy of the $Sr_2Cu_3O_4Cl_2$ crystal in the mean field approximation is well established[28,30,31] and can be written as follows:

$$\Phi_{\rm mag} = \int_V dV \Big\{ \frac{4}{M_0^2}\big[J_0(\mathbf{M}^2 - \mathbf{L}^2) + J_{\rm av}\mathbf{M}\cdot\mathbf{M}_{\rm F} + J_{\rm pd}\mathbf{M}_{\rm F}\hat{\sigma}_z\mathbf{L} + K_\perp L_z^2\big] - \frac{8}{M_0^4}K_\parallel L_x^2 L_y^2 - \mathbf{H}\cdot\mathbf{M}_{\rm F} - 2\mathbf{H}\cdot\mathbf{M}\Big\}. \quad (2)$$

Here V is the sample volume, M_0 is the CuI sublattice magnetization, and orthogonal axes x and y are parallel to the crystal directions [100] and [010], respectively (see Fig. 2). $\hat{\sigma}_z$ is the Pauli matrix. The meaning and values of the phenomenological constants are given in Table I. In the last column of this table all the constants are converted to Oe by division by sublattice magnetization $M_0 = 27.4$ Gs (that corresponds to spin $s = 1/2$ per CuI site).

Contributions $\Phi_{\rm stray}$ and $\Phi_{\rm dest}$ in Eq. (1) arise from the long-range dipole-dipole interactions of the magnetic and magnetoelastic nature, correspondingly, and depend upon the sample shape. In the experiments[26] the samples had a shape of a thin square or rectangular. Demagnetization and de-stressing effects in this case give rise to a rather complicated inhomogeneous spatial distribution of the effective magnetic and stress fields inside the sample. However, if the sample size is much greater than the characteristic width of the domain walls, the contribution of the fine-scale inhomogeneities into $\Phi_{\rm stray}$ and $\Phi_{\rm dest}$ is negligible. To this end the rectangular shape can be approximated with an ellipse with the same aspect ratio. So, for the sake of simplicity we consider a thin (thickness c) pillar with an elliptic cross section whose principal axes X and Y are parallel to $\langle 110\rangle$ directions within the Cu_3O_4 layers (see Fig. 2). In this case

$$\Phi_{\rm stray} = \frac{V}{2}\big[N_a^{\rm dm}\langle M_{\rm FX} + 2M_X\rangle^2 + N_b^{\rm dm}\langle M_{\rm FY} + 2M_Y\rangle^2\big], \quad (3)$$

where the brackets $\langle\ldots\rangle$ mean averaging over the sample volume. The components of demagnetization tensor $N_{a,b}^{\rm dm}$ are calculated in a standard way:[32]

$$N_a^{\rm dm} = \frac{4\pi c}{a\sqrt{1-k^2}}\int_0^{\pi/2}\frac{\sin^2\phi d\phi}{\sqrt{1-k^2\sin^2\phi}}; \qquad N_b^{\rm dm} = \frac{4\pi c\sqrt{1-k^2}}{a}\int_0^{\pi/2}\frac{\cos^2\phi d\phi}{\sqrt{1-k^2\sin^2\phi}}. \quad (4)$$

Here $a \geqslant b(\gg c)$ are the ellipses's semi-axes (parallel to the X and Y axes) and the parameter $k^2 = 1 - b^2/a^2$ depends upon an aspect ratio b/a of the sample.

The de-stressing energy be written in an analogous form[23]

$$\Phi^{\rm dest} = \frac{V}{M_0^4}\big[N_{\rm is}^{\rm des}\big(\langle L_Y^2 - L_X^2\rangle^2 + 4\langle L_X L_Y\rangle^2\big) + N_{\rm 2an}^{\rm des}\langle L_X^2 - L_Y^2\rangle - N_{\rm 4an}^{\rm des}\big(\langle L_X^2 - L_Y^2\rangle^2 - 4\langle L_X L_Y\rangle^2\big)\big]. \quad (5)$$

An explicit form of the de-stressing constants $N^{\rm des}$ depends upon the elastic and magnetoelastic properties of the crystal

TABLE I. Parameters used in the free energy potential [Eq. (2)]. The second column gives the raw data (in meV) as taken from Refs. 26, 30 and 31, in the last column the same values are given in Oe.

Parameter	Meaning	Value in meV	Value in Oe
J_0	CuI-CuII superexchange (in-plane)	130	$1.02\cdot 10^7$
$J_{\rm av}$	isotropic pseudodipolar interaction	-12	$-9.4\cdot 10^5$
$J_{\rm pd}$	anisotropic pseudodipolar interaction	-0.027	$-2.1\cdot 10^3$
$K_\perp$	out-of-plane anisotropy[28]	0.068	$5.3\cdot 10^3$
$K_\parallel$	in-plane anisotropy	$10\cdot 10^{-6}$	$7.8\cdot 10^{-2}$

which we assume to be isotropic (that means, in particular, the following relation between the elastic modules: $c_{11} - c_{12} = 2c_{44}$). Then,

$$N_{\rm is}^{\rm des} = \frac{\lambda^2(3-4\nu)}{16c_{44}(1-\nu)},$$
$$N_{2}^{\rm des} = \frac{c}{b}\cdot\frac{[\lambda^2(2-3\nu)+\lambda_v\lambda]J_2(k)}{8c_{44}(1-\nu)}, \qquad (6)$$
$$N_{\rm 4an}^{\rm des} = \frac{c}{b}\cdot\frac{\lambda^2 J_4(k)}{3c_{44}(1-\nu)},$$

where λ and λ_v are magnetoelastic constants, $\nu = c_{12}/(c_{11}+c_{12})$ is the Poisson ratio, and we have introduced the dimensionless shape-factors $J_{2,4}(k)$ as follows[23]

$$J_2(k) = \int_0^{\pi/2}\frac{(\sin^2\phi + \cos 2\phi/k^2)d\phi}{\sqrt{1-k^2\sin^2\phi}},$$
$$J_4(k) = \int_0^{\pi/2}\frac{(1-8\cos 2\phi - k^2\sin^2\phi + 8\cos 2\phi/k^2)d\phi}{\sqrt{1-k^2\sin^2\phi}}. \qquad (7)$$

In Eqs. (3) and (5) we have omitted the $Z(\|z\|[001])$ components of the demagnetizing and de-stressing tensors as inessential for further consideration.

Expressions (2), (3), and (5) can be substantially simplified if one takes into account that (i) far below the Néel temperature the values of sublattice magnetizations M_0 and $M_{\rm F}$ are saturated and constant; as a result (ii) $\mathbf{L}\perp\mathbf{M}$ and $\mathbf{L}^2+\mathbf{M}^2 = M_0^2$ (normalization conditions); (iii) if the magnetic field is much smaller than the spin-flip field, $H \ll J_0/M_0$ and coupling between the FM and AFM subsystems is much smaller than the AFM exchange $J_{\rm av}M_F \ll J_0M_0$, the magnetization induced in the AFM subsystem is small, $M \ll M_0$, and vector $\mathbf{M}$ can be excluded from Eq. (2) as follows:[33]

$$\mathbf{M} = \frac{1}{8J_0}\left\{\mathbf{L}\times\left[\left(\mathbf{H} - 2\frac{J_{\rm av}}{M_0^2}\mathbf{M}_{\rm F}\right)\times\mathbf{L}\right]\right\}; \qquad (8)$$

(iv) if out-of-plane anisotropy is strong enough, $K_\perp \gg K_\parallel$ (see Table I), all the magnetic vectors lie within xy (and, equivalently, XY) plane and could be described with the only angle variable, as shown in Fig. 2:

$$L_x = M_0\cos\theta, \quad L_y = M_0\sin\theta;$$
$$M_{{\rm F}x} = m_{\rm F}M_0\cos\varphi, \quad M_{{\rm F}y} = m_{\rm F}M_0\sin\varphi. \qquad (9)$$

Here $m_{\rm F}[=10^{-3}$ for $Sr_2Cu_3O_4Cl_2$ (Ref. 30)] is a dimensionless constant that represents the ratio between the spin moments localized on CuII and CuI sites.

With account of the relations (8) and (9) the specific potential $\phi \equiv \Phi/V$ [see Eq. (1)] takes the following form

$$\begin{aligned}\phi = {} & 4J_{\rm pd}m_{\rm F}\langle\cos(\theta+\varphi)\rangle + K_\parallel\langle\cos 4\theta\rangle - \frac{J_{\rm av}^2}{8J_0}m_{\rm F}^2\langle\cos 2(\theta-\varphi)\rangle \\ & - m_{\rm F}H\left[\left(1-\frac{J_{\rm av}}{8J_0}\right)\langle\cos(\varphi-\psi)\rangle + \frac{J_{\rm av}}{8J_0}\langle\cos(2\theta-\psi-\varphi)\rangle\right] + \frac{H^2}{32J_0}\langle\cos 2(\theta-\psi)\rangle \\ & - N_{\rm 2an}^{\rm des}\langle\cos 2(\theta-\psi)\rangle + \frac{1}{2}M_0m_{\rm F}^2\left[N_a^{\rm dm}\langle\cos(\varphi-\psi)\rangle^2 + N_b^{\rm dm}\langle\sin(\varphi-\psi)\rangle^2\right] \\ & + N^{\rm des}\langle\cos 2(\theta-\psi)\rangle^2 + \Delta N^{\rm des}\langle\sin 2(\theta-\psi)\rangle^2, \end{aligned} \qquad (10)$$

where ψ is an angle between the magnetic field and x axis, $N^{\rm des} \equiv N_{\rm is}^{\rm des} + N_{\rm 4an}^{\rm des}$, $\Delta N^{\rm des} \equiv 4(N_{\rm is}^{\rm des} - N_{\rm 4an}^{\rm des})$, and we assume that the field is parallel to one of the principal axes of the sample (this corresponds to the experimental situation that will be discussed below). Here and for the rest of the paper we use the values in Oe (see the last column of Table I) instead of energy units (say, $\phi \to \phi/M_0$, etc.).

Let us consider the case which corresponds to the experimental setup in Refs. 28 and 31, namely, the magnetic field is parallel to one of the easy axes, $\mathbf{H}\|[110]$, so, $\psi = \pi/4$. In an infinite sample (all the components of tensors $N^{\rm dm}, N^{\rm des}$ are equal to zero) the minimization of ϕ with respect to magnetic variables θ and φ gives rise to the four solutions labeled as A1,2 and B1,2 (see Fig. 2). Equilibrium values at $H = 0$ are

$$\begin{aligned} &\text{state A1}: \quad \theta_{\rm A1} = -\pi/4, \quad \varphi_{\rm A1} = \pi/4; \\ &\text{state B1}: \quad \theta_{\rm B1} = \pi/4, \quad \varphi_{\rm B1} = 3\pi/4; \\ &\text{state A2}: \quad \theta_{\rm A2} = 3\pi/4, \quad \varphi_{\rm A2} = 5\pi/4; \\ &\text{state B2}: \quad \theta_{\rm B2} = 5\pi/4, \quad \varphi_{\rm B2} = -\pi/4. \end{aligned} \qquad (11)$$

It should be stressed that, in contrast to pure AFM's, the configurations with $(\mathbf{M}_{\rm F},\mathbf{L})$ and $(\mathbf{M}_{\rm F},-\mathbf{L})$ are inequivalent due to anisotropic pseudodipolar interactions (described by the constant $J_{\rm pd}$).

Figure 4 illustrates the field-induced variation of equilibrium magnetic configurations (represented by X projections of $\mathbf{M}_{\rm F}$ and $\mathbf{L}$ vectors) obtained from the numerical minimization of Eq. (10) using the data from Table I. It is clearly seen that within the interval $|H| \leqslant H_{\rm s-fl} = 525$ Oe there exist all four states A1,2 and B1,2. The magnetic field removes degeneracy between the states A1, A2, and B,[34] as can be seen from Fig. 4(a). In particular, when $H \geqslant 0$, the specific partial energies $\phi_j \equiv \phi(\theta_j,\varphi_j)$ of equilibrium states are related as follows: $\phi_{\rm A1} < \phi_{\rm B} < \phi_{\rm A2}$. So, in some cases (discussed below) variation of the external field may induce formation of the AFM (B) instead of the FM (A2) domain. Orientations of $\mathbf{M}_{\rm F}$ and $\mathbf{L}$ vectors in the A states are not influenced by the field, while in the B states both vectors are slightly tilted [see Figs. 4(b) and (c)]. Rotation of AFM vector from the field direction in the state B (where $\mathbf{H}\|\mathbf{L}$) is a peculiar feature of the

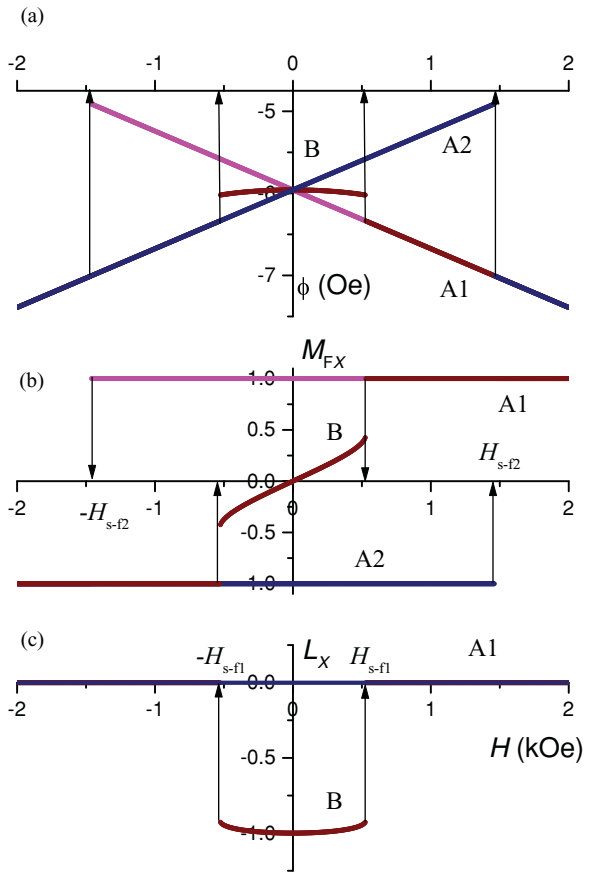

FIG. 4. (Color online) Stability ranges of homogeneous configurations shown in Fig. 2 in the external magnetic field $\mathbf{H}\|[110]$. (a) Specific energy (in Oe) of equilibrium homogeneous state vs H. (b, c) Normalized projections of FM and AFM moments on the field direction. Field induces rather noticeable rotation of $\mathbf{M}_F$ vector toward the (b) field direction and (c) slight tilt of $\mathbf{L}$ vector. Loss of stability takes place at the critical values $H = H_{s-f1,2}$, as shown with arrows.

FM + AFM multiferroic caused by pseudodipolar interactions between CuI and CuII ions. In the pure antiferromagnets an AFM vector $\mathbf{L}$ keeps parallel (with respect to $\mathbf{H}$) orientation up to the field of spin-flop transition.

The first critical field $H_{s-f1} \propto \sqrt{J_0 K_\parallel}$ corresponds to a step-like (spin-flop) transition B1,2 → A1. In the interval $H_{s-f1} < |H| < H_{s-f2} = 1465$ Oe the potential Φ has only two minima that correspond to the states A1 and A2. The second critical field H_{s-f2} corresponds to the 180° switching of the $\mathbf{M}_F$ vector. Its value depends on the effective anisotropy that originates from the pseudodipolar coupling (corresponding constants J_{av}, J_{pd}) and in-plane anisotropy $K_\parallel$ and can be calculated only numerically. Above $H \geqslant H_{s-f2}$ the sample is in a single domain state (A1).

We should also stress that the above calculations for homogeneous (single-domain sample) generalize a theoretical description of the magnetic state given in Ref. 31 in two aspects: account for mutual influence of CuI and CuII magnetizations and complete the description for all the domain types. Our analysis revealed metastable states (B1,2) in the field oriented along the [110] axis and also field-induced spin-flop transitions that are typical for AFM. However, in real, finite-size samples step-like variation of magnetization (and other macroscopic parameters) that accompanies spin-flop transition is usually smeared due to the multidomain structure. The details of such a behavior are considered in the next section.

III. EQUILIBRIUM DOMAIN STRUCTURE AND MAGNETIZATION CURVES

The magnetic structure of the finite-size sample can change due to the rotation of the magnetic moments and due to restructurization of the DS. Thus, on the large scales (much greater than the characteristic scale of the magnetic inhomogeneity, i.e., domain wall thickness) the magnetic structure is represented by a set of magnetic variables $\{\theta_j, \varphi_j\}$ that describe the orientation of FM and AFM vectors inside different domains (j = A1, A2, B1, B2) and a set of variables $\{\xi_j\}$ that represents the amount of matter (say, volume fraction) in the state of the j type (obviously, $\sum \xi_j = 1$). Equilibrium DS in the presence of the external field is then found from the condition for the minimum of Φ with respect to independent variables.

In such an approach one can neglect the contribution of the domain walls into the free energy potential Φ. However, we implicitly account for the inhomogeneities in the spatial distribution of the FM and AFM vectors when we chose independent variables for the potential Φ. Namely, the reconstruction of the DS may proceed in two ways: (i) by the field-induced motion of the domain walls; (ii) by the nucleation and growth of the energetically favorable domains. The first way is almost activation-less and the corresponding ξ_j are free variables, while in the second case the system should overcome the potential barrier related to the formation of the domain walls and the ξ_j values are fixed by the prehistory of the sample. In the case under consideration the domain walls between AFM (A/B) and FM (A1/A2 or B1/B2) domains have different energies, and so, appear at different conditions. In what follows we consider some typical situations and show the way to control the DS with the appropriate treatment of the sample.

A. Four types of domains

In the case when all four types of domains may freely grow or diminish in size (say, in a virgin sample that initially contains domains of all types), the external magnetic field is screened by an appropriate domain configuration (see Fig. 5) and the effective field inside the sample is zero. Formally it means that all the ξ_j are free variables. Equilibrium values of the magnetic variables in this case are given by Eq. (11) and the domain fractions depend on the magnetic field as follows:

$$\xi_{A1,A2} = \frac{1}{4}\left[1 - \xi^{(0)} \pm \frac{2H}{H_{dm}} + \left(\frac{H}{H_{des}}\right)^2\right];$$
$$\xi_{B1} = \xi_{B2} = \frac{1}{4}\left[1 + \xi^{(0)} - \left(\frac{H}{H_{des}}\right)^2\right], \quad (12)$$

where we have introduced the following notations

$$H_{dm} \equiv m_F N_a^{dm} M_0, \quad H_{des} \equiv 8\sqrt{J_0 N^{des}}. \quad (13)$$

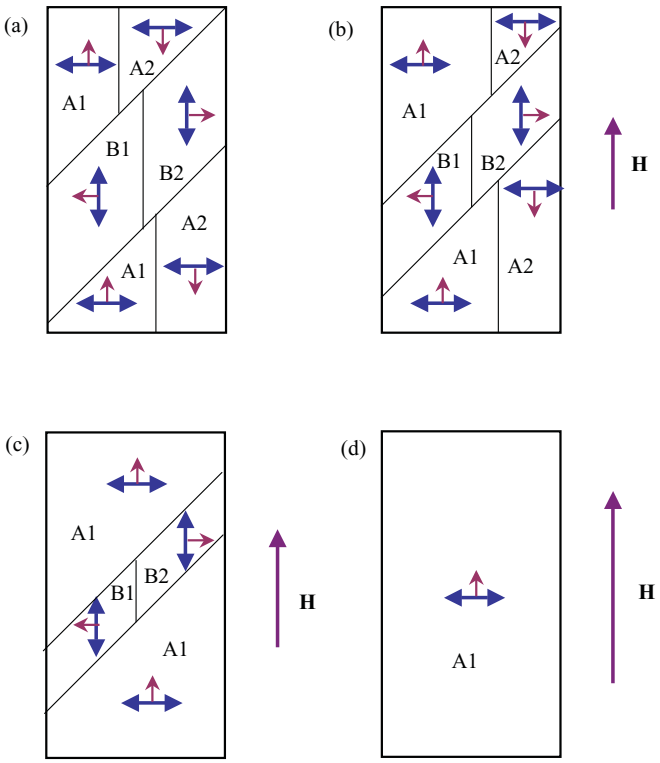

FIG. 5. (Color online) Behavior of the combined FM and AFM domain structures in the external magnetic field $\mathbf{H}\|[110]$ (parallel to the long side of the sample). (a) In the field absence all types of domains (A1, A2, B1, B2) are equally represented, the disbalance $\xi^{(0)}$ between type A and type B fractions depends upon the aspect ratio of the sample. (b) In the region $H \leqslant H_{\rm cr1}$, the domains are rearranged in such a way that the effective magnetic field vanishes. (c) In the interval $H_{\rm cr1} \leqslant H \leqslant H_{\rm cr2}$ the unfavorable domains of the A2 type disappear, A1 domains compete with the domains of the B type. (d) At $H > H_{\rm cr2}$ the sample is a single domain.

Physically, $H_{\rm dm}$ is the FM demagnetizing field calculated as if an AFM subsystem is absent. In an analogous way, $H_{\rm des}$ can be treated as a de-stressing field in the absence of FM ordering.

As seen from Eq. (13), the value of the de-stressing field is enhanced due to exchange interactions (constant J_0). On the contrary, the demagnetizing field is weakened due to the small FM moment ($m_{\rm F} \ll 1$). So, in the crystal under consideration the demagnetizing effects are much smaller than the de-stressing ones, $H_{\rm dm} \ll H_{\rm des}$ (see Table II).

The value $\xi^{(0)}$ introduced in Eq. (12) represents the disbalance between type A and type B domain fractions in the field absence. This value depends upon the shape of the sample [or, equivalently, upon the aspect ratio, see Eq. (6)]:

$$\xi^{(0)} \equiv \frac{N^{\rm des}_{\rm 2an}}{N^{\rm des}} \approx \frac{c}{b} J_2(k). \tag{14}$$

Such a shape-induced nonequivalence of domains has a magnetoelastic origin (see Ref. 23 for details) and originates from the AFM properties of the system. The disbalance between type A and type B domains was observed in the experiments in Ref. 26 for the different sample shapes. The value $\xi^{(0)} = 0.22$ calculated from Eq. (14) for the typical sample size (see Table II) fits well the experimental magnetization curves, as we will show below.

The described configuration of the DS [see Eq. (12)] is schematically shown in Fig. 5(b). The fraction of the unfavorable domains A2, B1, and B2 diminishes and at the critical value,

$$H = H_{\rm cr1} \equiv \frac{H^2_{\rm des}}{H_{\rm dm}} \left[1 - \sqrt{1 - (1 - \xi^{(0)}) \left(\frac{H_{\rm dm}}{H_{\rm des}} \right)^2} \right] \approx \frac{1}{2}(1 - \xi^{(0)}) H_{\rm dm}, \tag{15}$$

calculated from Eq. (12) on the condition that $\xi_{\rm A2} = 0$, the unfavorable FM domains A2 disappears.

At $H \geqslant H_{\rm cr1}$ the internal effective magnetic field is nonzero and magnetizations in the domains of the B type rotate. However, if $H_{\rm cr1} \ll H_{\rm s-f}$ (as, indeed is the case in the crystal under consideration), the small tilt of $\mathbf{M}_{\rm F}$ and $\mathbf{L}$ vectors can be neglected and the field dependence of the domain fractions [shown in Fig. 5(c)] is approximated as

$$\xi_{\rm A1} = \frac{1}{2} \left[1 - \xi^{(0)} + \frac{16 H m_{\rm F} J_0}{H^2_{\rm des}} + \left(\frac{H}{H_{\rm des}} \right)^2 \right], \qquad \xi_{\rm B1,2} = \frac{1}{4} \left[1 + \xi^{(0)} - \frac{16 H m_{\rm F} J_0}{H^2_{\rm des}} - \left(\frac{H}{H_{\rm des}} \right)^2 \right]. \tag{16}$$

TABLE II. Parameters used in numerical simulations. The source of data (experimental or calculated) is specified in the last column.

Parameter	Meaning	Value	Rem
$a \times b \times c$	Sample size	$7 \times 2 \times 0.5$ mm^3	Ref. 26
$m_{\rm F}$	$M_{\rm F}/M_0$	$7 \cdot 10^{-4}$	Ref. 28
$M_{\rm F}$	Saturation magnetization	$7 \cdot 10^{-3}$ emu/g	Ref. 26
$\xi^{(0)}$	Shape-induced bias	0.22	Eq. (14)
$H_{\rm dm}$	Demagnetization field	0.3 Oe	Eq. (13)
$N^{\rm des}$	Destressing const., $T = 120$ K	7 mOe	Fitting
	$T = 100$ K	1.5 mOe	param.
$H_{\rm des}$	Destressing field, $T = 120$ K	2.1 kOe	Eq. (13)
	$T = 100$ K	1.1 kOe	

The second critical field at which the unfavorable domains of the B type disappear [calculated from Eq. (12) on condition $\xi_{B1,2} = 0$] is given by the expression

$$H_{cr2} \equiv 8m_F J_0 \left[\sqrt{1 + \left(\frac{H_{des}}{8m_F J_0} \right)^2 \left(1 + \xi^{(0)}\right)} - 1 \right] \approx \frac{2N^{des}}{m_F}(1 + \xi^{(0)}). \quad (17)$$

Above this field, $H \geqslant H_{cr2}$, the sample is a single domain (A1) on average, with the possible remnants of the states A2 and B and the corresponding domain walls that can serve as nucleation centers during the field cycling. Full monodomainization of the sample takes place above the critical field $H_{s-f2} \gg H_{cr2}$ at which all the states except A1 became unstable.

Field cycling of the sample that initially had all the types of domains is reversible if the maximal field value H_{max} is not very large, $H_{cr2} \leqslant H_{max} \ll H_{s-f2}$. Macroscopic magnetization is parallel to the direction of the external field due to the full compensation of the perpendicular component by the B1 and B2 domains.

Field dependence of macroscopic magnetization $M_{par} \propto (\xi_{A1} - \xi_{A2})$ at $T = 120$ K calculated from Eqs. (12) and (16) (see Tables I and II) is represented in Fig. 6. One can distinguish three intervals that correspond to different domain composition: (i) steep growth of M_{par} from 0 to $\propto 0.5(1 - \xi^{(0)})M_F$ (at $H = H_{cr1}$) due to the motion of A1/A2 domain walls initiated by demagnetization; (ii) smooth growth of M_{par} from $\propto 0.5(1 - \xi^{(0)})M_F$ to $\approx M_F$ (at $H = H_{cr2}$) due to the motion of A1/B domain walls initiated by the de-stressing; (iii) very smooth growth of M_{par} due to the rotation of sublattice magnetizations (not seen in Fig. 6). Such a behavior contrasts with a "standard" magnetization curve of FM and also with the case when only two types of domains could compete under the action of the external field. The last case will be considered in detail in the next section.

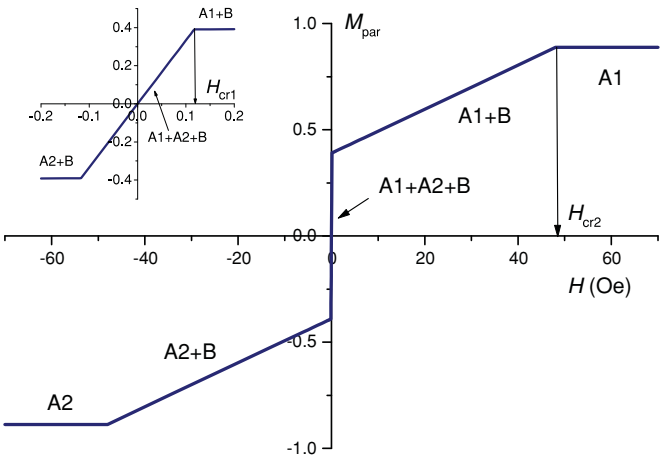

FIG. 6. (Color online) Magnetization curve (projection on field direction) in the external magnetic field $\mathbf{H} \| [110]$ for the case depicted in Fig. 5. Inset shows the details of magnetization behavior below H_{cr1}. The jogs (shown with arrows) arise at the critical fields $H = H_{cr1,2}$ when one type of domain disappears. Magnetization is normalized to saturation value.

B. Competition of two domains

Let us consider a sample that was preliminary monodomainized to the state A1 by excursion into the region of high field, $H \geqslant H_{s-f2}$. The DS in this case depends upon the relation between nucleation energies of different states. As it was shown above, at $H > 0$ an AFM domain B is more favorable than a FM domain A2 [see Fig. 4(a)]. If, in addition, there is a slight misalignment between the magnetic field **H** and a crystal axis [110] that removes degeneracy between the B1 and B2 states, the DS of the sample is represented by the domains of only two types, A1 and B1.

Equilibrium values of the magnetic variables in this case were calculated by numerical minimization of the potential (10) with limitations $\xi_{A2} = \xi_{B2} = 0$. The values of the de-stressing coefficient N^{des} at different temperatures (see Table II) were defined from the fitting of experimental data.[26]

Field dependence of the macroscopic magnetization at $T = 120$ K is shown in Fig. 7 with solid lines. The points represent experimental data.[26] Due to the fact that the domains

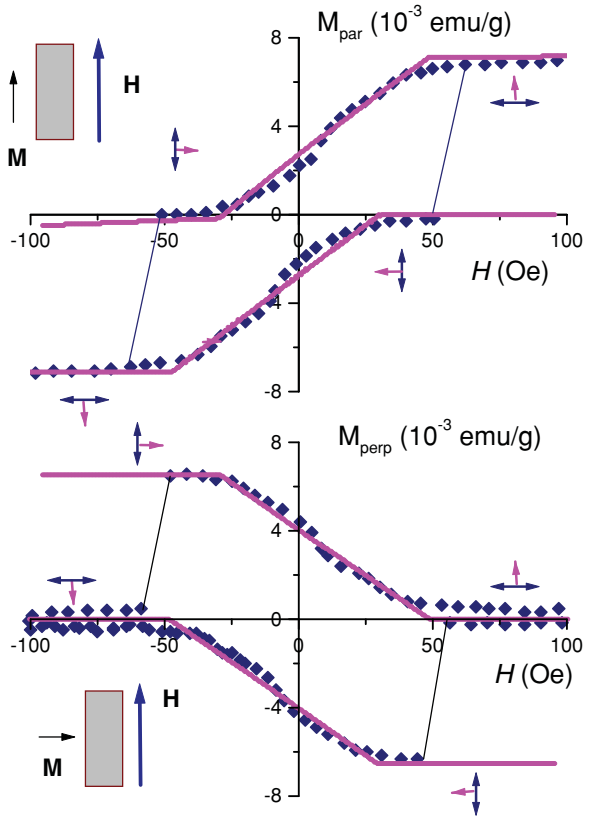

FIG. 7. (Color online) Macroscopic magnetization vs magnetic field. Points—experimental data for $Sr_2Cu_3O_4Cl_2$[26] taken at $T = 120$ K after monodomainization of the sample at high fields $H \propto 5$ T. Solid lines—theoretical approximation (see text for details). Upper and lower panels show, correspondingly, the parallel and perpendicular components of magnetization with respect to magnetic field. Insets show geometry of the experiment: orientation of the field with respect to the sample and orientation of the measured magnetization with respect to **H**. The dominant type of domains for each field interval is depicted schematically by the single- and double-headed arrows.

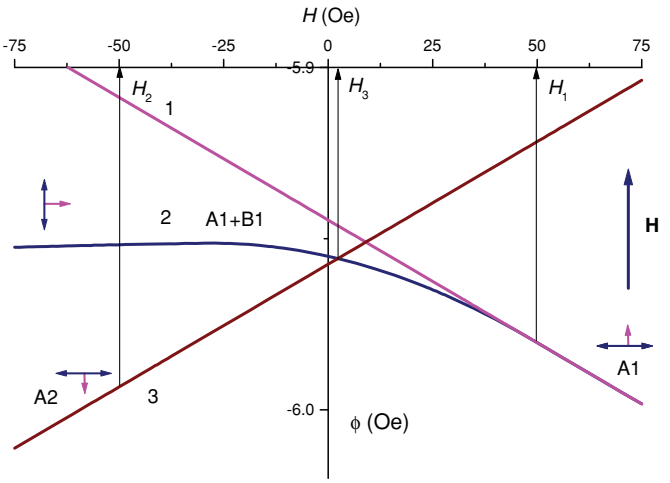

FIG. 8. (Color online) Magnetic energy *vs* magnetic field, $T = 120$ K. Lines 1 and 3 correspond to a single domain state (domains A1 and A2, correspondingly), line 2 represents equilibrium two-domain state (domains A1 and B1). Domain B1 appears at $H = H_1$. Domain A2 appears at field $H = H_2$ (determined empirically) when the energy difference between two- and single- domain states is enough for nucleation of this energetically favorable domain. At $H = H_3$ the energy of two-domain state is equal to the energy of a single-domain state A2, but the potential barrier between these two states prevents nucleation of the domain A2.

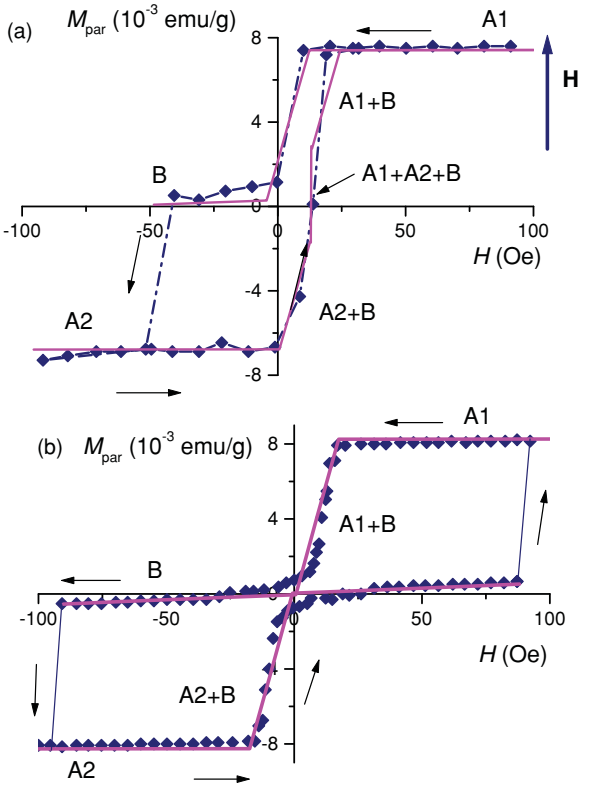

FIG. 9. (Color online) Macroscopic magnetization vs magnetic field for different field treatment. Points—experimental data for $Sr_2Cu_3O_4Cl_2$[26] taken at $T = 100$ K (see text for details), solid lines—theoretical approximations. Thin arrows show the direction of field sweeping. (a) Competition between FM and AFM domain structures. Field treatment starts from the high positive values ($H \approx 1$ T) where the sample is in a single-domain state. Variation of field is swept at intermediate value $|H_2| \leqslant |H| \ll |H_{cr2}|$, large enough to induce switching between metastable, B1, and stable, A2, states and small enough to remove the traces of A1 and B1 phases from the sample. (b) Hysteresis loop with the excursion into high fields. For any field value the DS includes only two types of domains, as in Fig. 7. Only the parallel component of magnetization is shown.

A1 and B1 cannot screen the external field, the macroscopic magnetization has two components: one that is parallel to **H** (upper panel in Fig. 7) and one that is perpendicular to **H** (lower panel). The parallel and perpendicular components represent the fractions of the A1 and B1 domains, respectively.

When the field decreases from high positive values, an AFM domain of the B type appears and magnetizations $M_{\text{par}}(\mathbf{H})$ and $M_{\text{perp}}(\mathbf{H})$ vary smoothly between zero and saturation value. The slope of magnetization curves depends upon the de-stressing coefficient and is thus much smaller than the initial steep slope in the four-domain case (see Fig. 6). At small negative field the sample is almost a single domain (type B). However, this state is a metastable one from the energy point of view, as seen from Figs. 4(a) and 8. Really, below $H = H_3 \approx 2.8$ Oe (marked with an arrow in Fig. 8) the energy of the state A2 (with $\mathbf{M}_F \uparrow\downarrow \mathbf{H}$) is lower than that of a single domain state B1 and a multidomain state A1 + B1. On the other hand, due to preliminary high-field treatment, the sample contains no nucleation centers of the A2 state. So, the states B1 and A2 are separated with the potential barrier that could be overcome only at $H = H_2 \approx -50$ Oe (according to Ref. 26, this value varies from sample to sample and depends on temperature). After the subsequent excursion into high negative fields (well below H_2) the sample transforms into a single domain A2 and one can observe competition between the A2 and B2 domains during the further field increase.

C. Domain structure and field treatment

In the previous sections we have considered two limiting cases of field treatment that result in two types of magnetization curves. In the virgin sample (no field treatment) the magnetization can be smoothly and reversibly changed between two opposite directions. Field cycling between high fields (high enough to remove all the domain walls and the remains of unfavorable domains) results in a hysteretic behavior when magnetization varies smoothly between zero and saturation value and then suddenly changes due to the transition from metastable to stable state.

In this section we consider some intermediate case when a single domain sample is cycled in low fields. The corresponding magnetization curve is shown in Fig. 9(a) (solid lines—numerical simulations, points—experimental data[26] $T = 100$ K). Field cycling starts at high positive fields, where the sample is a single domain. When the field is decreased down to $H = H_1$ [see Fig. 8(a)] the domains of the B1 type appear and the DS consists of A1 and B1 domains. The magnetization curve [upper curve in Fig. 9(a)] in this case is of the two-domain type discussed in Sec. III B (we still assume the slight misalignment that excludes one type of B domain). However, further behavior of the DS, and hence magnetization, depends upon the size of the loop. If the loop is small ($|H| \leqslant |H_2|$, where H_2 is a coercive field

at which domain B1 transforms into A2 as explained above), magnetization varies smoothly between zero value at negative fields and saturation value at positive fields. If the loop is very large ($|H| \geqslant |H_{cr2}|$), the DS structure consists of two domains: A1 and B1 for large positive and small negative fields and A2 and B2 for large negative and small positive fields, as shown in Figs. 7 and 9(b). In the intermediate case ($|H_2| \leqslant |H| \ll |H_{cr2}|$) the DS includes three types of domains, A1, A2, and B2 [lower curve in Fig. 9(a)], and the magnetization curve is asymmetric. It is worth noting that theoretical magnetization curves calculated with only one fitting parameter (de-stressing coefficient N^{des}) fit well to the experimental data, as seen from Figs. 7 and 9.

IV. DISCUSSION

We have considered the different types of the DS behavior in a multiferroic with AFM and FM order parameters. First of all, it is instructive to summarize the general features of DS behavior that are different in single and multiferroics.

(1) In multiferroic (in contrast to single ferroics) the potential barriers between different pairs of states (A1–A2 and A1–B1 in our case) can differ significantly due to the different physical nature of the varying order parameter. As a result, one can easily control the types of domains that form the DS and corresponding macroscopic properties of the sample.

(2) One of the important, experimentally observed characteristics of the multidomain sample is the value critical field at which some types of domains disappear. Our calculations show that the critical fields of the same nature in multiferroics and single ferroics depend upon phenomenological constants in a different way. For example, in an AFM single ferroic the critical field $H_{des} \propto \sqrt{J_0 N^{des}}$, while in the AFM + FM multiferroic corresponding field $H_{cr} \propto N^{des}/m_F$ [see Eq.(17)].

(3) In multiferroics the shape-dependent constants (like demagnetizing, depolarizing, or de-stressing coefficients) can be not only of a different physical nature, but also, which is important, have different tensor and symmetry properties. This opens a way to control the DS by the combination of the external fields of a different symmetry (e.g., magnetic and stress fields, etc). In addition, it may result in an unusual field dependence of macroscopic parameters, like the appearance of perpendicular magnetization of the sample described above.

Second, some features of the DS behavior may result from the peculiarities of order parameters. In a particular case of $Sr_2Cu_3O_4Cl_2$ multiferroic we found that depending on the field treatment the DS may include from one to four types of domains and can be unambiguously determined from the magnetization curves in the field $\mathbf{H}\|[110]$. Namely, if DS includes all types of domains, macroscopic magnetization is parallel to $\mathbf{H}$, the magnetization curve is reversible, varies between $\pm$ saturation value, and includes a steep section at small fields. If the DS consists of three types of domains (A1, A2, and B1) the macroscopic magnetization has two components, parallel, M_{par}, and perpendicular, M_{perp}, to $\mathbf{H}$. During field cycling M_{par} varies between positive and negative saturation values, while M_{perp} varies between zero and saturation value. At last, if the DS includes only two domains, A and B, both M_{par} and M_{perp} vary between zero and saturation value.

It should be mentioned that the nontrivial magnetization behavior of $Sr_2Cu_3O_4Cl_2$ was interpreted in Ref. 26 as resulting from restructurization of the DS. However, the proposed phenomenological model was based on the idea that the thermodynamic stability of DS is due to the entropy contribution from the domain walls[35] and effective steric repulsion between them.

We argue that the formation of the equilibrium AFM domain structure results from the de-stressing effect which, in turn, originates from magnetoelastic interactions. An absolute value of the magnetoelastic constant is rather small (compared to such AFM's as NiO, $KCoF_3$, etc) and corresponds to the spontaneous strain $u \propto 10^{-6}$ (for the estimation we took $c_{44} = 20$ GPa at $T = 120$ K). Such a small value of u explains the low potential barrier for the formation of AFM domains.

The analysis of magnetization curves shows that low-field susceptibility χ of the sample that consists of AFM domains is inversely proportional to the de-stressing coefficient N^{des} (in contrast to FM, where χ depends upon the demagnetization constant). According to the experiments,[26] the inverse susceptibility χ^{-1} of $Sr_2Cu_3O_4Cl_2$ shows nontrivial temperature dependence [see Fig. 10(b)] and attains the

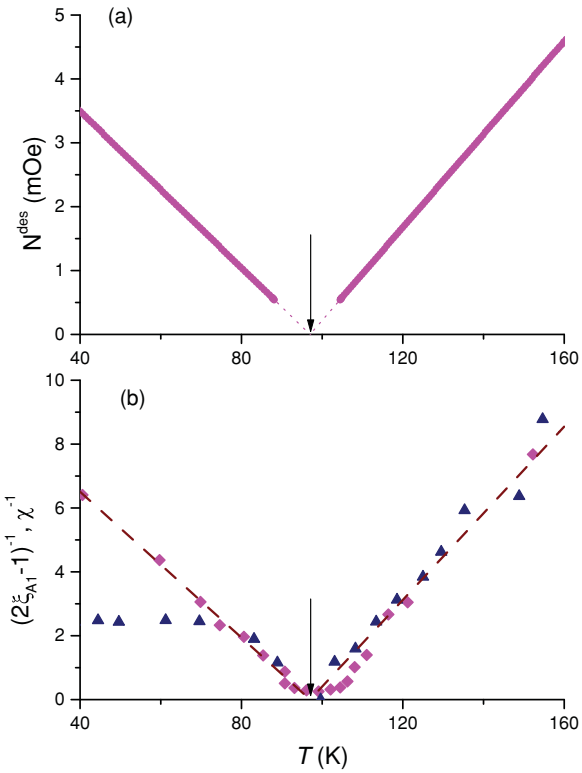

FIG. 10. (Color online) Temperature dependence (a) of the destressing coefficient N^{des} predicted from the comparison with the (b) temperature dependence of the reciprocal domain A1 fraction $(2\xi_{A1} - 1)^{-1}$ (triangles) and the inverse susceptibility χ^{-1} (diamonds) plotted according to data.[26] Raw data for χ^{-1} were normalized (multiplied by the appropriate factor) to fall into the same range of values as $(2\xi_{A1} - 1)^{-1}$. Dashed line shows linear approximation of the experimental data. Peculiarity at $T = 97$ K is indicated with the arrow.

minimum at $T = T_0 = 97$ K. The domain fraction ξ_{A1} at fixed **H** extracted from the neutron scattering experiments[26] shows the same temperature dependence as χ, as can be seen from Fig. 10(b). Using correlation between N^{des} and χ we can predict the following temperature dependence of the de-stressing coefficient depicted in Fig. 10(a):

$$N^{\text{des}}(T) = \begin{cases} 7.3 \cdot 10^{-5} \cdot (T - T_0), & T \geqslant T_0, \\ 6.13 \cdot 10^{-5} \cdot (T_0 - T), & T < T_0. \end{cases} \quad (18)$$

If one takes into account that $N^{\text{des}} \propto \lambda^2/c_{44}$ [see Eq. (6)] it is possible also to anticipate a peculiarity of the elastic (or magnetoelastic) properties of the crystal in the vicinity of $T = T_0$. The magnetoelastic nature of AFM domains in $Sr_2Cu_3O_4Cl_2$ may reveal itself in the stress-induced magnetization of the sample. In particular, we expect the same behavior as shown in Fig. 6 of the parallel and perpendicular magnetization under mechanical tension/contraction along [110] in the presence of the small demagnetizing field ($\propto H_{\text{dm}} \propto 0.3$ Oe).

At last, we would like to outline a possible generalization of the considered model to the description of the DS in multiferroics which combine magnetic and ferroelectric ordering (see, e.g., Ref. 17). The main idea of the presented approach is to account for the long-range interactions of the elastic (magnetoelastic) nature via de-stressing energy (5). In the general case, an additional (compared to demagnetizing) shape-dependent contribution into the free energy of the sample originates from the long-range interactions between the "elastic dipoles" induced by magnetic, ferroelectric, and/or martensitic phase transition:[23]

$$\Phi^{\text{dest}} = \frac{V}{2}\langle\sigma^{\text{in}}_{jl}\rangle\aleph_{jklm}\langle\sigma^{\text{in}}_{km}\rangle, \qquad \aleph_{jklm} \equiv \frac{\partial^2}{\partial r_k \partial r_m}\int_V G_{jl}(\mathbf{r} - \mathbf{r}')d\mathbf{r}', \quad (19)$$

where $G_{km}(\mathbf{r} - \mathbf{r}')$ is a Green's function of elasticity (with zero nonsingular part) and fourth rank symmetrical de-stressing tensor $\hat{\hat{\aleph}}$ depends upon the sample shape. An explicit expression for the transition-induced internal stresses $\hat{\sigma}^{\text{in}}$ depends upon the character of the ordering. In particular, for AFM $\sigma^{\text{in}}_{jk} = \lambda_{jlkm} L_l L_m$, where the fourth order tensor λ_{jlkm} describes magnetoelastic coupling. In the case of magnetoelectrical systems $\hat{\sigma}^{\text{in}}$ can be proportional to the combination of piezoelectric, $\hat{\lambda}^{\text{piezo}}$ and magnetoelastic, $\hat{\lambda}^{\text{m-e}}$ constants, for example,

$$\hat{\sigma}^{\text{in}} = \hat{\lambda}^{\text{piezo}} \cdot \mathbf{P} + \hat{\lambda}^{\text{m-e}} : \mathbf{L} \otimes \mathbf{L}. \quad (20)$$

Further consideration of the DS depends upon the symmetry of the crystal and of the particular sample. It should be underlined that the de-stressing energy (19) takes into account the contribution of the domains with noncollinear orientation of polarization/magnetization and could not be reduced to depolarizing/demagnetizing effects.

In summary, we described the possible scenario of field-induced restructurization of the domains in the system that consists of the domains of a different physical nature. The proposed model can be extended to multiferroics that show simultaneously ferroelectric and AFM ordering and also to FM martensites with ferroelastic and ferromagnetic ordering.

ACKNOWLEDGMENTS

The authors acknowledge the financial support from the Department of Physics and Astronomy of the National Academy of Sciences of Ukraine in the framework of the Special Programme for Fundamental Research. The work was partially supported by a grant from the Ministry of Education and Science of Ukraine.

*malyshen@ukrpack.net

[1] S. Cheong and M. Mostovoy, Nature Mat. **6**, 13 (2007).
[2] M. Gajek, M. Bibes, S. Fusil, K. Bouzehouane, J. Fontcuberta, A. Barthelemy, and A. Fert, Nature Mat. **6**, 296 (2007).
[3] C. R. dela Cruz, B. Lorenz, Y. Y. Sun, C. W. Chu, S. Park, and S.-W. Cheong, Phys. Rev. B **74**, 180402(R) (2006).
[4] V. A. Chernenko, A. Amengual, E. Cesari, V. V. Kokorin, and I. K. Zasimchuk, J. Phys. IV France **05**, C2-95 (1995).
[5] R. Ramesh and N. A. Spaldin, Nature Mat. **6**, 21 (2007).
[6] Y.-H. Chu, L. W. Martin, M. B. Holcomb, and R. Ramesh, Materials Today **10**, 16 (2007).
[7] R. de Sousa and J. E. Moore, J. Nanoelectron. Optoelectron. **3**, 77 (2008).
[8] M. Fiebig, T. Lottermoser, D. Fröhlich, A. V. Goltsev, and R. V. Pisarev, Nature (London) **419**, 818 (2002).
[9] T. Zhao, A. Scholl, F. Zavaliche, K. Lee, M. Barry, A. Doran, M. P. Cruz, Y. H. Chu, C. Ederer, N. A. Spaldin, R. R. Das, D. M. Kim, S. H. Baek, C. B. Eom, and R. Ramesh, Nature Mat. **5**, 823 (2006).
[10] N. Balke, S. Choudhury, S. Jesse, M. Huijben, Y. H. Chu, A. P. Baddorf, L. Q. Chen, R. Ramesh, and S. V. Kalinin, Nature Nanotechnol. **4**, 868 (2009).
[11] D. Meier, N. Leo, M. Maringer, T. Lottermoser, M. Fiebig, P. Becker, and L. Bohatý, Phys. Rev. B **80**, 224420 (2009).
[12] Y. Tokunaga, N. Furukawa, H. Sakai, Y. Taguchi, T. Arima, and Y. Tokura, Nature Mat. **8**, 558 (2009).
[13] T. Kordel, C. Wehrenfennig, D. Meier, T. Lottermoser, M. Fiebig, I. Gélard, C. Dubourdieu, J. W. Kim, L. Schultz, and K. Dörr, Phys. Rev. B **80**, 045409 (2009).
[14] S. H. Baek, H. W. Jang, C. M. Folkman, Y. L. Li, B. Winchester, J. X. Zhang, Q. He, Y. H. Chu, C. T. Nelson, M. S. Rzchowski, X. Q. Pan, R. Ramesh, L. Q. Chen, and C. B. Eom, Nature Mat. **9**, 309 (2010).
[15] W. Eerenstein, M. Wiora, J. L. Prieto, J. F. Scott, and N. D. Mathur, Nature Mat. **6**, 348 (2007).
[16] A. Poole, P. J. Brown, and A. S. Wills, J. Phys. Conf. Ser. **145**, 012074 (2009).
[17] S. Seki, H. Murakawa, Y. Onose, and Y. Tokura, Phys. Rev. Lett. **103**, 237601 (2009).

[18]C. Kittel, Rev. Mod. Phys. **21**, 541 (1949).
[19]M. B. Holcomb, L. W. Martin, A. Scholl, Q. He, P. Yu, C. H. Yang, S. Y. Yang, P. A. Glans, M. Valvidares, M. Huijben, J. B. Kortright, J. Guo, Y. H. Chu, and R. Ramesh, Phys. Rev. B **81**, 134406 (2010).
[20]C. Yaicle, C. Martin, Z. Jirak, F. Fauth, G. André, E. Suard, A. Maignan, V. Hardy, R. Retoux, M. Hervieu, S. Hébert, B. Raveau, C. Simon, D. Saurel, A. Brûlet, and F. Bourée, Phys. Rev. B **68**, 224412 (2003).
[21]V. Hardy, S. Majumdar, S. J. Crowe, M. R. Lees, D. M. Paul, L. Hervé, A. Maignan, S. Hébert, C. Martin, C. Yaicle, M. Hervieu, and B. Raveau, Phys. Rev. B **69**, 020407 (2004).
[22]V. G. Baryakhtar, A. N. Bogdanov, and D. A. Yablonskii, Phys. Usp. **31**, 810 (1988).
[23]H. V. Gomonay and V. M. Loktev, Phys. Rev. B **75**, 174439 (2007).
[24]Z. V. Gareeva and A. K. Zvezdin, Phys. Status Solidi Rapid Res. Lett. **3**, 79 (2009).
[25]Z. V. Gareeva and A. K. Zvezdin, Europhys. Lett. **91**, 47006 (2010).
[26]B. Parks, M. A. Kastner, Y. J. Kim, A. B. Harris, F. C. Chou, O. Entin-Wohlman, and A. Aharony, Phys. Rev. B **63**, 134433 (2001).
[27]S. Noro, T. Kouchi, H. Harada, T. Yamadaya, M. Tadokoro, and H. Suzuki, Mater. Sci. Eng. B **25**, 167 (1994).
[28]Y. J. Kim, R. J. Birgeneau, F. C. Chou, M. Greven, M. A. Kastner, Y. S. Lee, B. O. Wells, A. Aharony, O. Entin-Wohlman, I. Y. Korenblit, A. B. Harris, R. W. Erwin, and G. Shirane, Phys. Rev. B **64**, 024435 (2001).
[29]According to Ref. 30, the FM moments at CuII ions result from the anisotropic "pseudodipolar" interactions between CuI and CuII.
[30]M. A. Kastner, A. Aharony, R. J. Birgeneau, F. C. Chou, O. Entin-Wohlman, M. Greven, A. B. Harris, Y. J. Kim, Y. S. Lee, M. E. Parks, and Q. Zhu, Phys. Rev. B **59**, 14702 (1999).
[31]F. C. Chou, A. Aharony, R. J. Birgeneau, O. Entin-Wohlman, M. Greven, A. B. Harris, M. A. Kastner, Y. J. Kim, D. S. Kleinberg, Y. S. Lee, and Q. Zhu, Phys. Rev. Lett. **78**, 535 (1997).
[32]A. I. Akhiezer, V. G. Bar'yakhtar, and S. V. Peletminskii, *Spin Waves*, North-Holland Series in Low Temperature Physics, Vol. 1, (North-Holland, Amsterdam, 1968).
[33]A. M. Kosevich, B. A. Ivanov, and A. S. Kovalev, *Nonlinear Magnetization Waves. Dynamical and Topological Solitons* (Naukova Dumka, Kiev, 1983), p. 192.
[34]States B1 and B2 are equivalent in the field parallel to the [110] direction.
[35]Y.-Y. Li, Phys. Rev. **101**, 1450 (1956).